NACA

RESEARCH MEMORANDUM

PERFORMANCE CHARACTERISTICS OF CANARD-TYPE MISSILE WITH WING-MOUNTED NACELLE ENGINES AT MACH NUMBERS 1.5 TO 2.0

By Emil J. Kremzier and Joseph Davids

Lewis Flight Propulsion Laboratory
Cleveland, Ohio

NATIONAL ADVISORY COMMITTEE
FOR AERONAUTICS

WASHINGTON

November 24, 1952

NATIONAL ADVISORY COMMITTEE FOR AERONAUTICS

RESEARCH MEMORANDUM

PERFORMANCE CHARACTERISTICS OF CANARD-TYPE MISSILE WITH WING-MOUNTED NACELLE ENGINES AT MACH NUMBERS 1.5 to 2.0

By Emil J. Kremzier and Joseph Davids

SUMMARY

The over-all performance characteristics of a complete canard-type missile configuration with wing-mounted nacelle engines were investigated in the Lewis 8- by 6-foot supersonic wind tunnel at Mach numbers of 1.5, 1.8, and 2.0. The investigation covered model angles of attack from 0° to 10°, control-surface-deflection angles from -6° to 10°, and a range of engine mass-flow ratios at a Reynolds number of approximately 8.0×10^6 based on wing mean aerodynamic chord.

Results of the investigation indicated that the addition of the engines to the no-engine configuration increased the lift and the drag but decreased the maximum lift-drag ratio to 5.2 at the design Mach number of 2.0 for zero control-surface deflection. The variation of the maximum lift-drag ratio with Mach number was very small. Increment of lift due to the engines was greater than the sum of the theoretically predicted isolated engine lifts, while the drag increment of the engines was approximately equal to the sum of the theoretical engine drags. Addition of the engines also produced a stabilizing effect on the pitching moment of the configuration about the reference moment center.

Increases in configuration drag with increasing mass-flow spillage resulted largely from the increases in engine additive drag, indicating that no major interference effect of mass-flow spillage on configuration drag existed.

Use of a constant-area section at the engine subsonic-diffuser entrance increased the range of stable operation but decreased the pressure recovery. Effects of control-surface deflection on engine mass flow and pressure recovery were negligible at zero angle of attack and caused only slight reductions at angle of attack.

INTRODUCTION

In the design of a complete missile configuration, many possible locations of the engine or engines exist with respect to the rest of the configuration. Fuselage-contained engines with side inlets, wing-mounted nacelle engines, and strut-mounted nacelle engines are several possibilities usually considered. The performance of a missile with two nacelle engines strut-mounted to the fuselage in a vertical plane at a rearward body station and having a canard-type wing-control-surface arrangement was investigated in reference 1. The performance of a similar type missile having two wing-mounted nacelle engines is investigated herein. The over-all force and moment characteristics of the configuration together with the diffuser performance of the engines as affected by the missile components were studied.

The investigation was conducted in the Lewis 8- by 6-foot supersonic wind tunnel at Mach numbers of 1.5, 1.8, and 2.0 for a range of angles of attack, control-surface deflections, and engine mass-flow ratios. The Reynolds number of the investigation was approximately 8.0×10^6 based on the wing mean aerodynamic chord.

SYMBOLS

b wing span, 52 in.

C_D drag coefficient, $\frac{D}{q_0 S}$

C_L lift coefficient, $\frac{L}{q_0 S}$

C_M pitching-moment coefficient about body station 58, $\frac{\text{moment}}{q_0 S \bar{c}}$

c local wing chord at spanwise station y.

$\bar{c}$ mean aerodynamic chord of wing, $\frac{\int_0^{\frac{b}{2}} c^2 dy}{\int_0^{\frac{b}{2}} c \, dy} = 17.97$ in.

D drag, lb

L lift, lb

M	Mach number
m	mass flow, slugs/sec
$\frac{m}{m_{ref}}$	mass-flow ratio, unity when free-stream tube as defined by cowl lip enters engine
$\left(\frac{m}{m_{ref}}\right)_t$	over-all mass-flow ratio, $\frac{(m)_1 + (m)_2}{(m_{ref})_1 + (m_{ref})_2}$
P/P_0	engine diffuser total-pressure recovery, ratio of total pressure at diffuser exit to free-stream total pressure
p	static pressure
q_0	free-stream dynamic pressure, $\frac{\gamma p_0 M_0^2}{2}$
S	total wing plan-form area, 900 sq in. (including projected areas blanketed by body and engines)
y	distance along wing in spanwise direction measured from fuselage center line
α	model angle of attack, deg
γ	ratio of specific heats, 1.4
δ	canard-control-surface deflection from body center line, positive deflection same sense as positive angle of attack

Subscripts:

d	refers to engine diffuser exit
max	maximum
0	free stream
1	refers to engine 1
2	refers to engine 2

APPARATUS AND PROCEDURE

A sketch of the model investigated with pertinent dimensions is shown in figure 1. The model was identical to that of reference 1 except that the nacelle engines were located on the wing. The fuselage consisted of a symmetrical body of revolution pointed at both ends and having a fineness ratio of 12 and a maximum diameter of 9 inches.

Plan area of the wing was 6.25 square feet, aspect ratio 3.0, taper ratio 0.5, and the 50-percent chord line was unswept and mounted on the body center line at station 69.75 inches. The airfoil section was a double circular arc, 5 percent thick.

The control surface was similar to the wing, with the exception that the thickness was increased to 8 percent near the root for structural reasons. Total plan area was 135 square inches, or 15 percent of the total wing area. The all-movable control surface was hinged about its 50-percent chord line and was remotely operated. The nose portion of the body adjacent to the forward half of the control surface was fixed to and deflected with the surface.

Two simulated ram-jet engines were mounted on the wing, one on either side of the body, with their center lines $2\frac{1}{2}$ engine diameters from and in a horizontal plane through the body center line. Sketches of engines 1 and 2, mounted on the starboard and port sides of the fuselage, respectively, are shown in figures 2 and 3. The contours of the two engines differ somewhat, but their effect on the missile performance was considered similar to that of two identical engines. An alternate centerbody was designed for engine 1, which changed the subsonic-diffuser area distribution (engine 1A, fig. 4) to provide an essentially constant subsonic-diffuser area for approximately the first six inches of diffuser length. Engine 2 had approximately the same subsonic-diffuser area distribution as engine 1 (fig. 4). Both engines have 25°-half-angle conical spikes. The spike tip projection of engine 1 is such that the oblique shock from the tip at the design Mach number of 2.0 falls slightly ahead of the cowl lip, while the tip projection of engine 2 is such that the oblique shock intersects the lip. Coordinates for the cowl and centerbody of engines 1 and 1A are given in table I.

Mass flow through the engines was varied by means of movable tailpipe plugs attached to a twin plug assembly which was supported by an auxiliary strut mounted independently of the model and the tunnel balance system.

Lift and drag forces of the combined model and support strut were measured on the tunnel balance system. An internal strain-gage balance, which measured model normal force, axial force, and pitching moment,

was located at the junction between the model and the support strut. The drag interference of the support strut on the model was included in the strain-gage measurements, but was believed to be quite small; therefore, no attempt was made to correct for it. Because of questionable accuracy of the strain-gage drag forces at angle of attack, a support-strut tare drag was obtained at zero angle of attack from the difference between the tunnel balance and internal strain-gage balance forces. This tare drag was then assumed constant with angle of attack at a given free-stream Mach number and used in conjunction with the tunnel balance-system drag to obtain model drag. While the above technique may admittedly introduce inaccuracies in the model drag at angle of attack, these inaccuracies are considered to be sufficiently small that they have no appreciable effect on the results of this report.

A slight negative lift measured on the tunnel balance system at angle of attack α and control-surface deflection δ of 0° was believed to result from model support-strut interference. Accordingly, the lift curves were shifted by a constant amount at each Mach number so that the curve for $\delta = 0^\circ$ would pass through zero lift at $\alpha = 0^\circ$.

Drags were obtained by averaging corresponding positive and negative angle-of-attack drag values from the tunnel balance system corrected for support-strut tare drag. Drag values for angles of attack between -6° and -10° were unobtainable because of limitations in the travel of the angle-of-attack mechanism; consequently, the fairing of the curves in this angle-of-attack range was somewhat arbitrary.

Pitching moments were obtained from internal strain-gage measurements and were shifted by a constant amount at each Mach number so that the curve for $\delta = 0^\circ$ passed through zero pitching moment at zero angle of attack.

Each engine contained an internal flow-straightening honeycomb located approximately 27.7 inches from the cowl lip and extending downstream about 5 inches. One three-tube static-pressure rake and three wall static-pressure orifices were located at cowl stations 25.7 and 37.7 inches in both engines.

Engine mass flow was determined from the known open area at the exit and the combustion-chamber static pressure, with the assumption that the exit area was choked. Diffuser total-pressure recovery was calculated from the known mass flow and the diffuser-exit static pressure.

In the reduction of the data, the forces and moments developed by the engine internal flow were removed from the measured values. The lift and drag components of the forces contributed by the engine internal flow were computed from the engine thrust. In the determination of the

moment developed by the internal flow through the engines, the assumption was made that the momentum change due to the turning of the entering free-stream tube occurred at the cowl lip.

The investigation was conducted at free-stream Mach numbers of 1.5, 1.8, and 2.0; model angles of attack of 0°, 3°, 6°, and 10°; control-surface-deflection angles of -6°, -3°, 0°, 5°, and 10°; and engine mass-flow ratios usually ranging from supercritical to the minimum value at which stable flow was obtained (hereafter called "minimum stable"). The Reynolds number of the investigation was approximately 8.0×10^6 based on the mean aerodynamic chord of the wing.

Reflected shock waves from the tunnel walls were believed to have a negligible effect on model forces at a free-stream Mach number of 2.0, since only a small part of the model was in this region. At a Mach number of 1.5, however, a somewhat larger portion of the model was in the reflected shock region, and some error may be present in the model forces. These errors are not considered to have any appreciable effect on the general trends of the curves presented, although the magnitudes may be slightly incorrect.

DISCUSSION OF RESULTS

Over-all Force and Moment Evaluation (Supercritical Operation)

Configuration lift coefficient for supercritical inlet flow as a function of angle of attack is presented in figure 5 for three free-stream Mach numbers and three control-surface-deflection angles. The dashed curves are for the configuration without engines with zero control-surface deflection and were obtained from reference 1. The slopes of the configuration lift curves are seen to decrease with increasing Mach number; while increasing the control-surface deflection did not affect the slope, but merely shifted the curves upward slightly. Addition of the engines increased the lift of the no-engine configuration about 12 percent in all cases presented.

Drag coefficients (supercritical) are presented in figure 6 for three Mach numbers and three control-surface-deflection angles. Dashed curves for the configuration without engines are also included for zero control-surface deflection. Configuration drag coefficient increased with decreasing Mach number and increasing control-surface deflection. Drag increases resulting from the addition of the engines ranged from about 23 percent at Mach 2.0 to about 44 percent at Mach 1.5 for zero angle of attack and zero control-surface deflection.

The slopes of the pitching-moment coefficient curves (supercritical) about station 58 are negative throughout the range of the investigation (fig. 7). As the free-stream Mach number is increased, the slopes become

less negative. For the configuration without engines (dashed curves), the slopes of the pitching-moment curves are only slightly negative, which indicates a decrease in static longitudinal stability about the reference moment center when the engines are removed or when the free-stream Mach number is increased.

The effects of the addition of the engines and of control-surface deflection on the variation of configuration lift-drag ratio with angle of attack is shown for three Mach numbers in figure 8. Maximum lift-drag ratio $(L/D)_{max}$ decreases with increasing control-surface deflection, and for zero control-surface deflection $(L/D)_{max}$ decreases slightly with increasing Mach number. Addition of the engines also caused a decrease in $(L/D)_{max}$. For most cases, $(L/D)_{max}$ occurred at an angle of attack of approximately 5°; and for free-stream Mach number M_0 of 2.0, a value of $(L/D)_{max}$ of 5.2 was obtained. The corresponding control-surface-deflection angle for trim at $\alpha = 5^{\circ}$ is on the order of 2° (fig. 7), which gives very little reduction in $(L/D)_{max}$ from the $\delta = 0^{\circ}$ value.

Effect of Engines on Configuration Performance

(Supercritical Operation)

The summation of the theoretical and experimental drags for the configuration components without engines as obtained from reference 1 is presented in figure 9 as a function of free-stream Mach number. Also included are the sum of the theoretical isolated engine drags and the decrease in theoretical wing drag resulting from the blanketing of a portion of the wing by the engines. In addition, experimental drag (supercritical) for the complete configuration is shown. The theoretical pressure and friction drags of the body were obtained from references 2 and 3, respectively. Pressure drag of the control surface and wing was determined from two-dimensional potential flow theory, and the tip effects were estimated from reference 4. The friction drag of these components was determined from reference 3. Engine pressure drag was obtained from linearized potential theory for engine 1 and from reference 5 for engine 2. Friction drag for both engines was also determined from reference 3. Values of engine additive drag were obtained from reference 6 where applicable.

Summation of the theoretical drags of the various isolated components of the configuration (fig. 9) results in overprediction of the drag of the complete configuration. If the theoretical drag of that portion of the wing blanketed by the engines is subtracted, however, the resultant agreement between experiment and theory is good. This good agreement is to a large extent coincidental, since the underprediction of the net increase in drag due to the addition of the engines compensates for the cumulative errors in the drag predictions of each of the other components.

Incremental lift resulting from the addition of the engines is shown in figure 10 for three Mach numbers and three control-surface-deflection angles. Theoretical lift curves for the sum of the lifts of the isolated engines obtained from the method of reference 7 modified to apply to an open-nosed body are also shown and are considered to be a fairly accurate indication of the experimental lifts of the isolated engines, based on a comparison of the experimental and theoretical curves of reference 8. Thus the incremental lift due to the engines (fig. 10) is considerably greater than the lift of the isolated engines, which indicates the presence of some favorable lift interference between the engines and the rest of the configuration.

The increment of configuration drag due to the engines is presented in figure 11 for three control-surface-deflection angles at each Mach number investigated. Theoretical engine drags at zero angle of attack were obtained from figure 9, and the drag increase with angle of attack was obtained from the drag component of the normal force as evaluated from reference 7 (lift and normal force are approximately equal for angles of attack up to 10°). In the lower angle-of-attack range, control-surface deflection had practically no effect on the drag contribution of the engines. For higher angles of attack, some variation in drag with control-surface deflection is shown but may be the result of the arbitrary fairing of the complete configuration drag curves in this region. Agreement between experiment and theory is fairly good, particularly in the lower angle-of-attack range. It should be pointed out, however, that agreement between experiment and theory cannot be expected, because the experimental values are for the engine in the presence of the rest of the configuration and contain effects of aerodynamic interference. The fact that fair agreement between experiment and theory is obtained indicates that the interference drag between the engines and the rest of the configuration is approximately equal to the drag of that portion of the wing blanketed by the engines.

Effect of Variation of Engine Mass-Flow Ratio on Configuration and Inlet Performance

The effects of variation of engine mass-flow ratio on the lift, drag, and pitching moment were investigated and, for the case of model drag, are presented in figure 12 for several angles of attack, three Mach numbers, and zero control-surface deflection.

Drag increases associated with decreases in over-all mass-flow ratio can be attributed largely to the increase in additive drag of the engines, which indicates that there is no major interference effect of engine mass-flow spillage on configuration drag. At a given free-stream Mach number,

increment of drag due to angle of attack is essentially independent of mass-flow ratio.

Configuration lift and pitching moment were found to be independent of engine mass-flow ratio at any given angle of attack or free-stream Mach number. The negligible effect of the variation of engine mass-flow ratio on pitching moment might be expected, however, in view of the fact that the engine inlets were located very close to the axial body station about which moments were taken.

2708

Variation of engine diffuser pressure recovery with mass-flow ratio is presented in figures 13, 14, and 15 for Mach numbers of 1.5, 1.8, and 2.0, respectively. Several angles of attack and control-surface-deflection angles are shown for each Mach number. Also shown are lines of constant diffuser-exit Mach number, M_d.

Except for $M_0 = 1.5$, the minimum mass-flow ratio shown on each curve represents the "minimum stable" point for that inlet. At the design Mach number of 2.0 for zero angle of attack (fig. 15(a)), engine 1A exhibited a greater range of stable operation than engine 1, but also had about 2 percent less total-pressure recovery. Thus the constant-area section near the throat of the subsonic diffuser was effective in increasing the range of stable operation of the inlet but also caused an increase in subsonic-diffuser friction losses which resulted in reduction of maximum pressure recovery.

The higher pressure recovery obtained with engine 1 as compared to that obtained with engine 2 (about 6 percent at design conditions) probably arose from the fact that the contours of engine 1 were designed so that the internal cowl-lip angle was tangent to the local entering flow direction at design conditions. The cowl and centerbody were then curved back very gradually to the direction of flow in the subsonic diffuser. On engine 2 the turning of the flow at the inlet entrance was very abrupt, and the associated turning losses were probably the cause for the measured reduction in pressure recovery.

At a free-stream Mach number of 1.5 (fig. 13), maximum pressure recoveries of engines 1 and 2 are comparable, which indicates a certain amount of insensitivity of inlet performance to cowl-lip angle and associated local centerbody curvature at lower Mach numbers. The subsonic-diffuser area variation of engine 1A continued to affect inlet performance at the lower Mach numbers, however, exhibiting a maximum pressure recovery several percent lower than that of engine 1 at a free-stream Mach number of 1.5.

Control-surface deflection had a negligible effect on engine mass flow and pressure recovery at all Mach numbers for zero angle of attack.

At angle of attack, however, slight decreases in engine mass flow and pressure recovery with increases in control-surface deflection were noted.

SUMMARY OF RESULTS

An investigation of the performance characteristics of a complete missile configuration having a canard-type wing-control-surface arrangement with two wing-mounted nacelle engines was conducted at Mach numbers of 1.5 to 2.0, and the following results were obtained:

1. Addition of the engines to the configuration increased the lift and the drag, but decreased the maximum lift-drag ratio. For zero control-surface deflection, maximum lift-drag ratio decreased slightly with increasing free-stream Mach number, and a value of 5.2 was obtained at a Mach number of 2.0.

2. The increase in configuration lift due to the presence of the engines was approximately 12 percent, and was considerably higher than the theoretically predicted isolated engine lift, which indicated some favorable engine configuration lift interference.

3. Increment of drag due to the engines was approximately equal to the sum of the theoretical drags of the isolated engines.

4. A stabilizing effect on the pitching moment about the reference moment center (station 58) was also noted from the addition of the engines.

5. The use of a constant-area section for the first $1\frac{1}{2}$ inlet diameters of engine subsonic-diffuser length increased the range of stable operation, but decreased the pressure recovery slightly.

6. Slight decreases in engine mass flow and pressure recovery with increasing control-surface deflection were noted only at angle of attack.

Lewis Flight Propulsion Laboratory
National Advisory Committee for Aeronautics
Cleveland, Ohio

REFERENCES

1. Obery, Leonard J., and Krasnow, Howard S.: Performance Characteristics of Canard-Type Missile with Vertically Mounted Nacelle Engines at Mach Numbers 1.5 to 2.0. NACA RM E52H08, 1952.

2. Jones, Robert T.: Estimated Lift-Drag Ratios at Supersonic Speeds. NACA TN 1350, 1947.

3. Tucker, Maurice: Approximate Calculation of Turbulent Boundary-Layer Development in Compressible Flow. NACA TN 2337, 1951.

4. Nielsen, Jack N.: Effect of Aspect Ratio and Taper on the Pressure Drag at Supersonic Speeds of Unswept Wings at Zero Lift. NACA TN 1487, 1947.

5. Jack, John R.: Theoretical Wave Drags and Pressure Distributions for Axially Symmetric Open-Nose Bodies. NACA TN 2115, 1950.

6. Sibulkin, Merwin: Theroetical and Experimental Investigation of Additive Drag. NACA RM E51B13, 1951.

7. Allen, H. Julian: Estimation of the Forces and Moments Acting on Inclined Bodies of Revolution of High Fineness Ratio. NACA RM A9I26, 1949.

8. Esenwein, Fred T., and Valerino, Alfred S.: Force and Pressure Characteristics for a Series of Nose Inlets at Mach Numbers from 1.59 to 1.99. I - Conical Spike All-External Compression Inlet with Subsonic Cowl Lip. NACA RM E50J26, 1951.

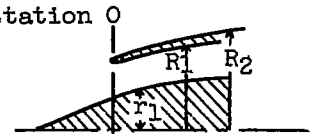

TABLE I - COORDINATES FOR ENGINES 1 AND 1A

(Dimensions in inches)

Cowl station	R_1	R_2	r_1[a]	r_{1A}[b]
-2.45	-----	-----	0	0
0.0	2.020	-----	1.142	1.142
0.5	2.135	2.200	1.258	1.360
1.0	2.250	2.330	1.490	1.540
1.5	2.340	2.425	1.600	1.675
2.0	2.410	2.495	1.662	1.775
2.5	2.460	2.550	1.710	1.840
3.0	2.500	2.590	1.740	1.900
3.5	2.530	2.625	1.762	1.937
4.0	2.560	2.650	1.770	1.970
4.5	2.580	2.670	1.760	1.995
5.0	2.600	2.690	1.750	2.012
5.5	Straight	Straight	1.746	2.040
6.0	↓	↓	1.738	2.060
6.5			1.727	2.075
7.0			1.721	2.090
7.5			1.713	2.100
8.0			1.705	2.105
8.5			1.695	2.112
9.0			1.685	2.115
10.0			1.670	2.125
11.0			1.645	2.112
12.0			1.625	2.090
13.0			1.600	2.060
14.0			1.570	2.010
15.0			1.530	1.945
16.0			1.487	1.865
17.0			1.438	1.765
18.0			1.375	1.650
19.0			1.300	1.525
20.0			1.220	1.375
21.0	↓	↓	1.125	1.213
22.28	3.09	3.18	1.000	1.000

[a]Centerbody 1.

[b]Centerbody 1A.

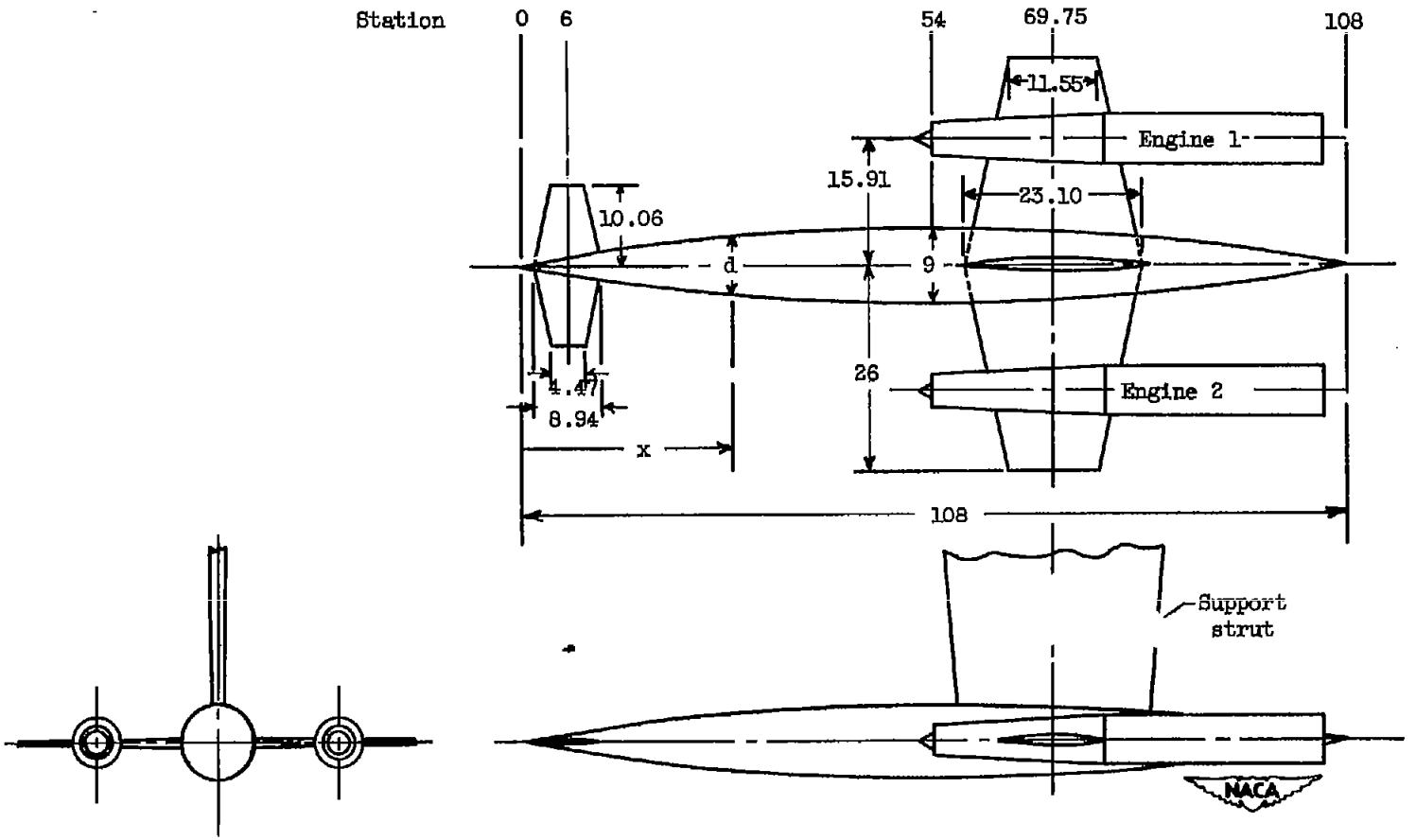

Figure 1. - Sketch of model investigated. Body defined by $d = 9\left[1 - \left(1 - \frac{x}{54}\right)^2\right]^{\frac{3}{4}}$. All dimensions are in inches.

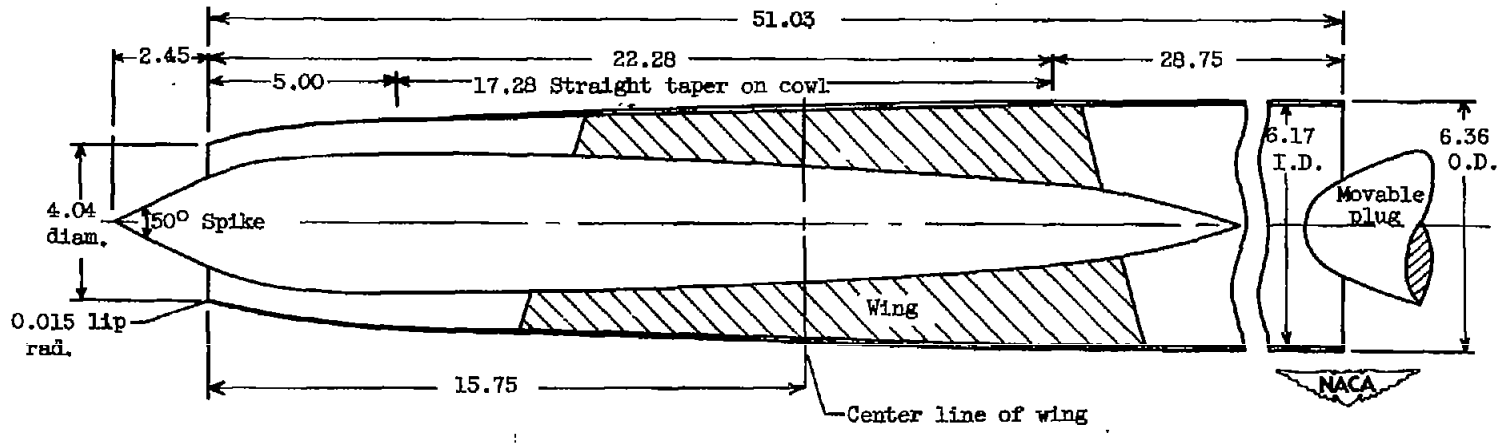

Figure 2. - Sketch of engine 1. Dimensions are in inches. For coordinates of cowl and centerbody, see table I.

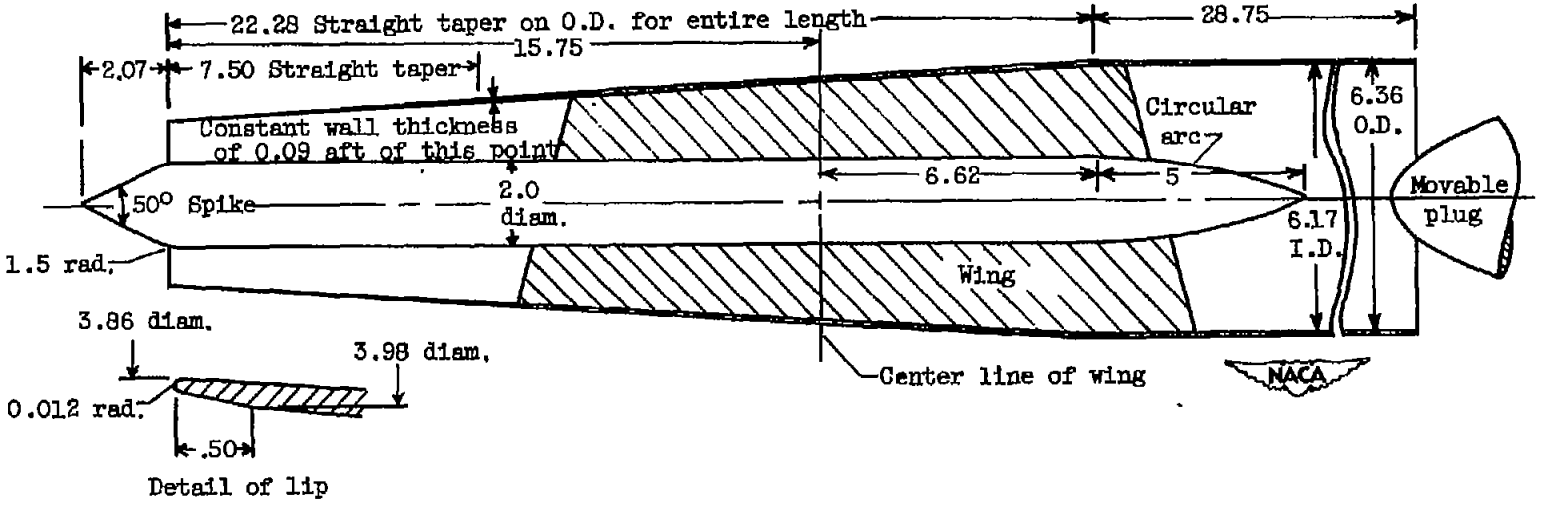

Figure 3. - Sketch of engine 2. Dimensions are in inches.

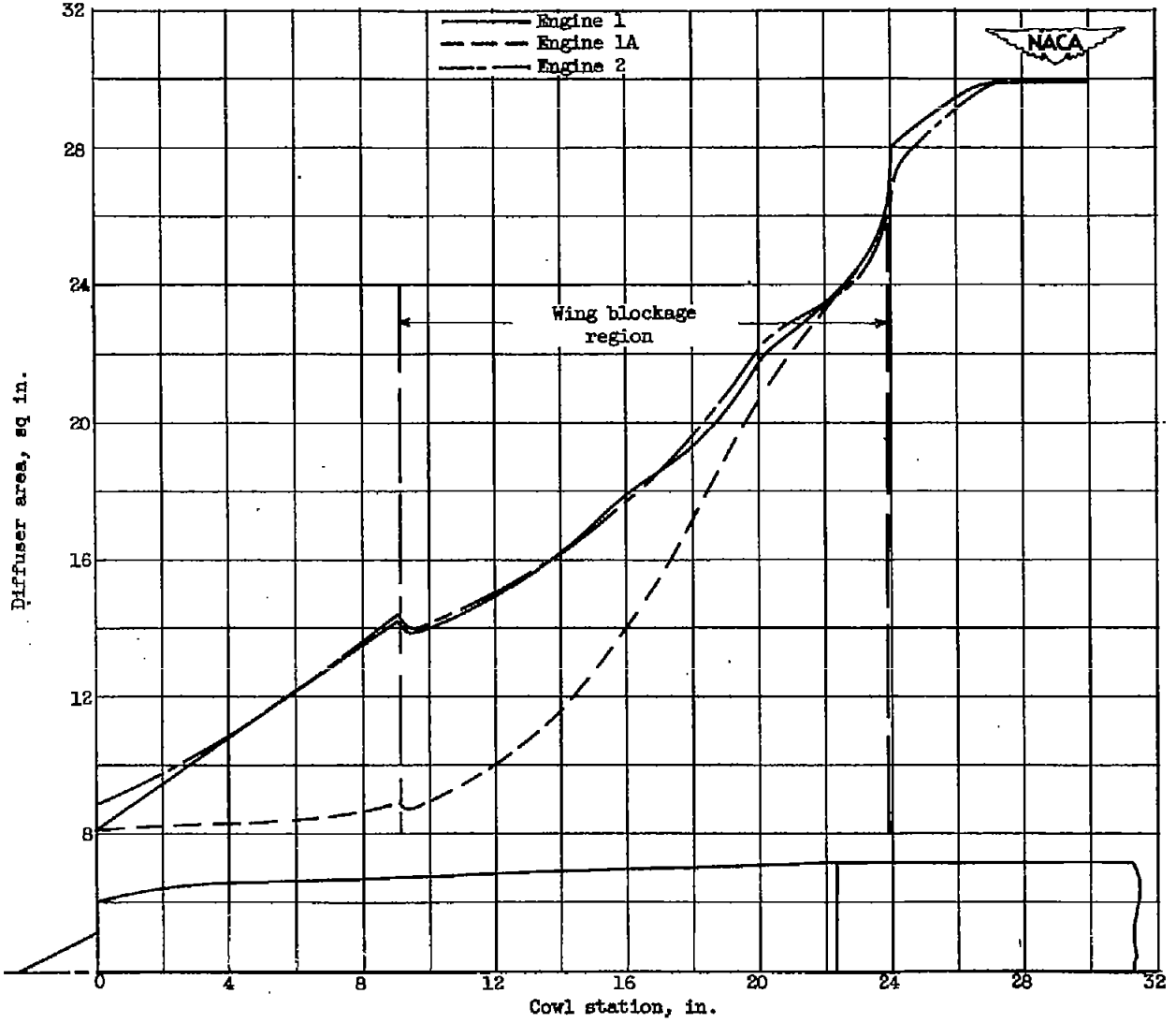

Figure 4. - Engine subsonic-diffuser area distribution.

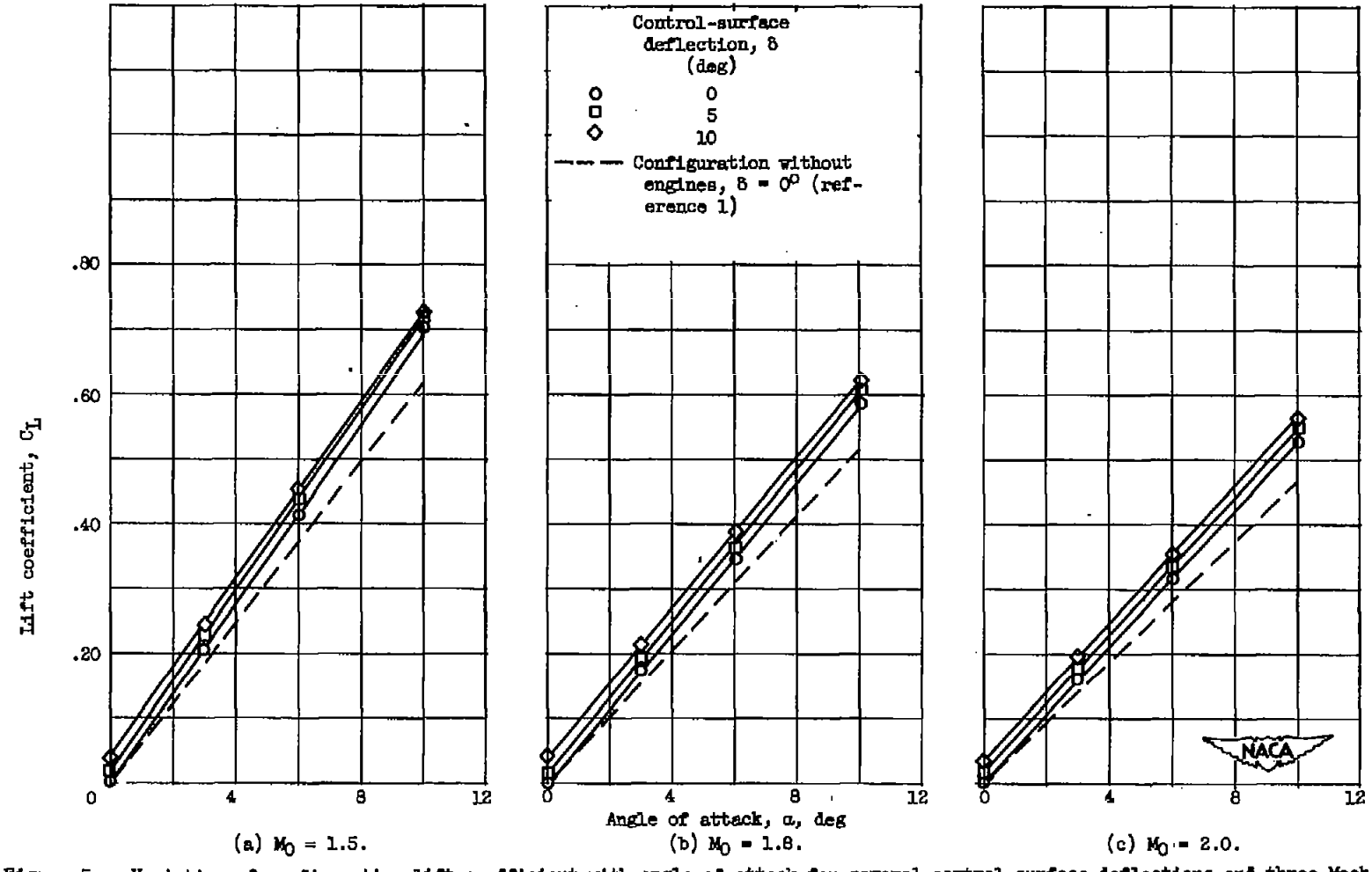

(a) M_0 = 1.5. (b) M_0 = 1.8. (c) M_0 = 2.0.

Figure 5. - Variation of configuration lift coefficient with angle of attack for several control-surface deflections and three Mach numbers. (Supercritical inlet operation.)

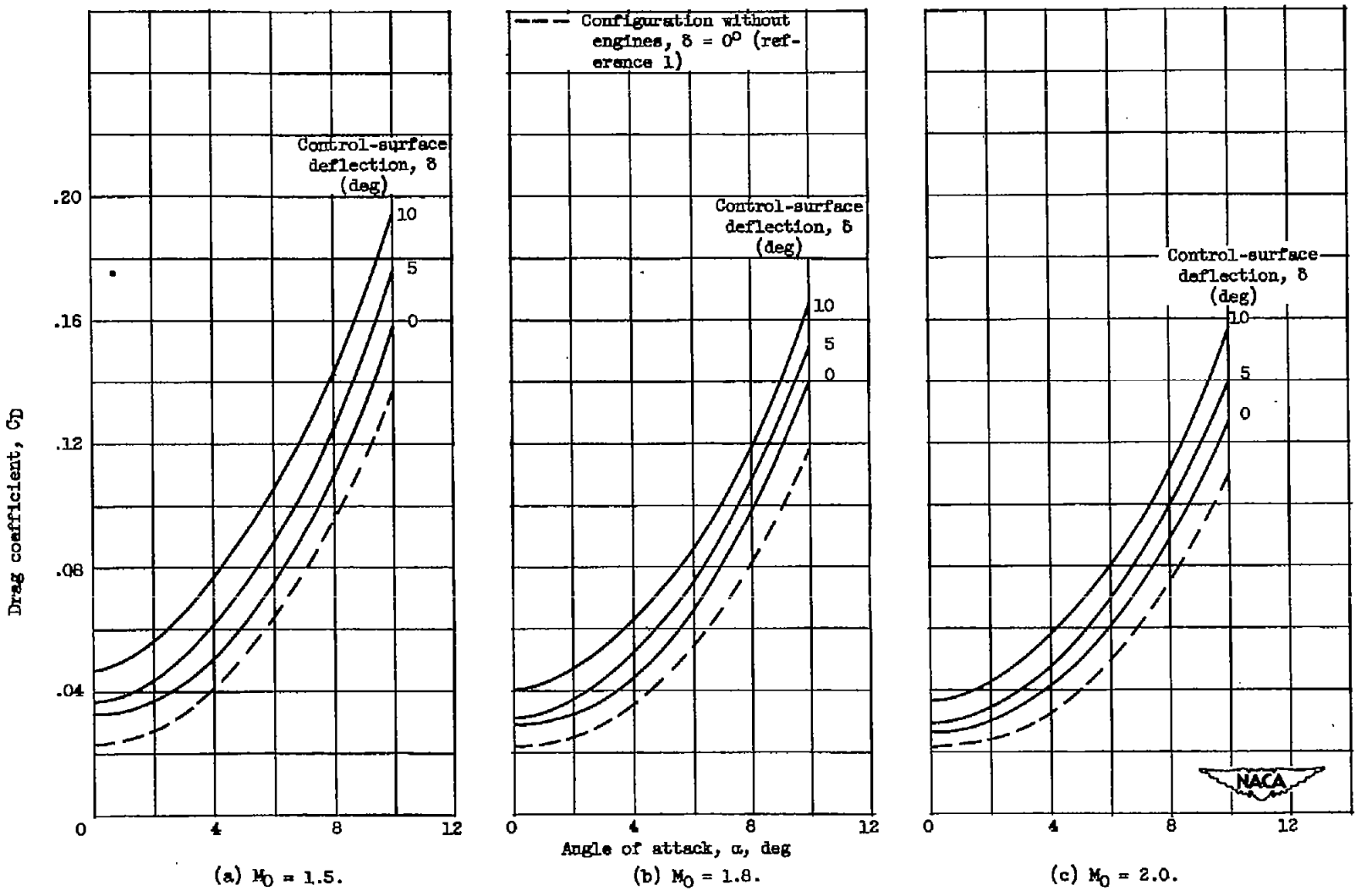

Figure 6. - Variation of configuration drag coefficient with angle of attack for several control-surface deflections and three Mach numbers. (Supercritical inlet operation.)

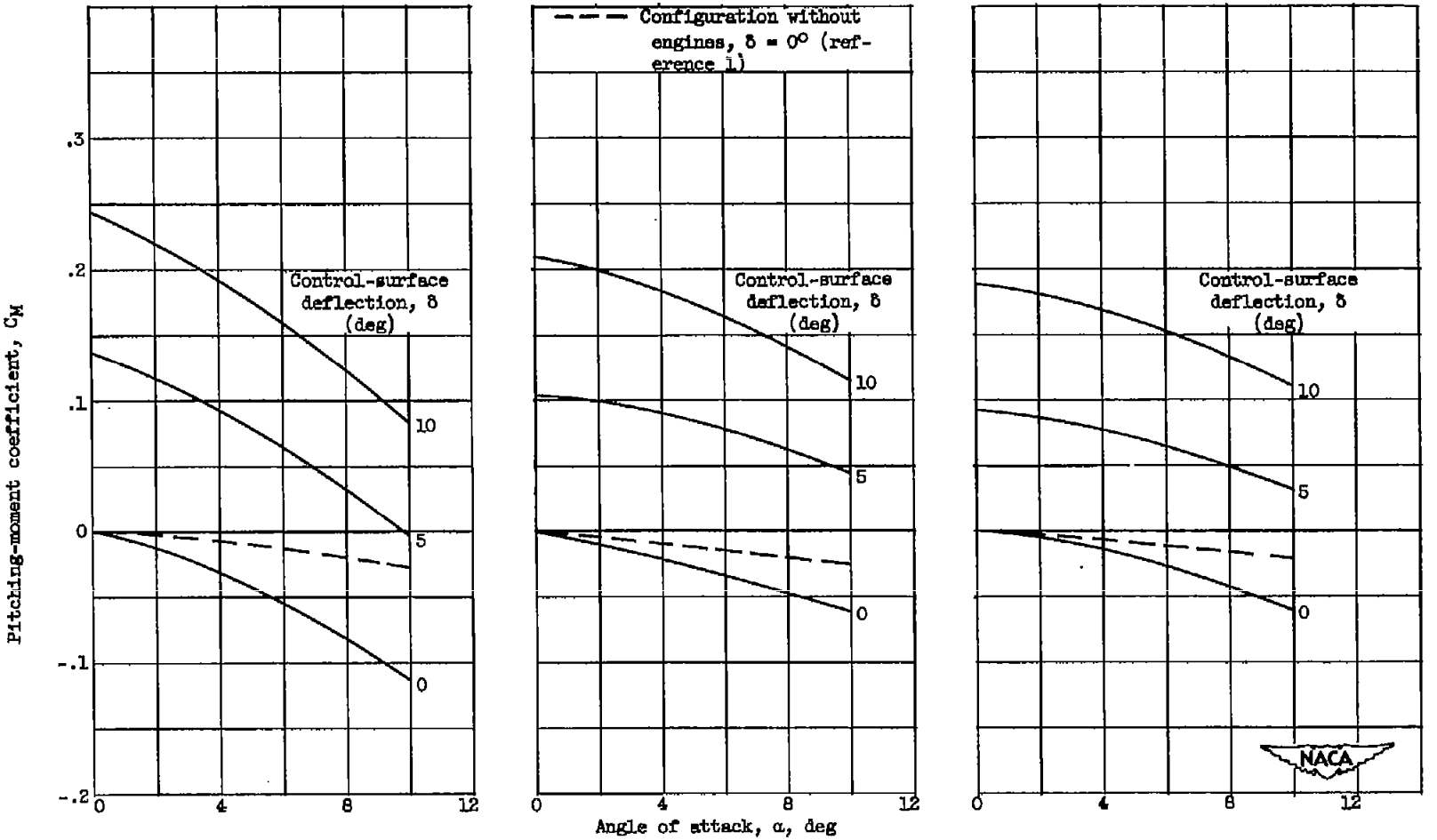

(a) $M_0 = 1.5$. (b) $M_0 = 1.8$. (c) $M_0 = 2.0$.

Figure 7. - Variation of configuration pitching-moment coefficient with angle of attack for several control-surface deflections and three Mach numbers. (Supercritical inlet operation.)

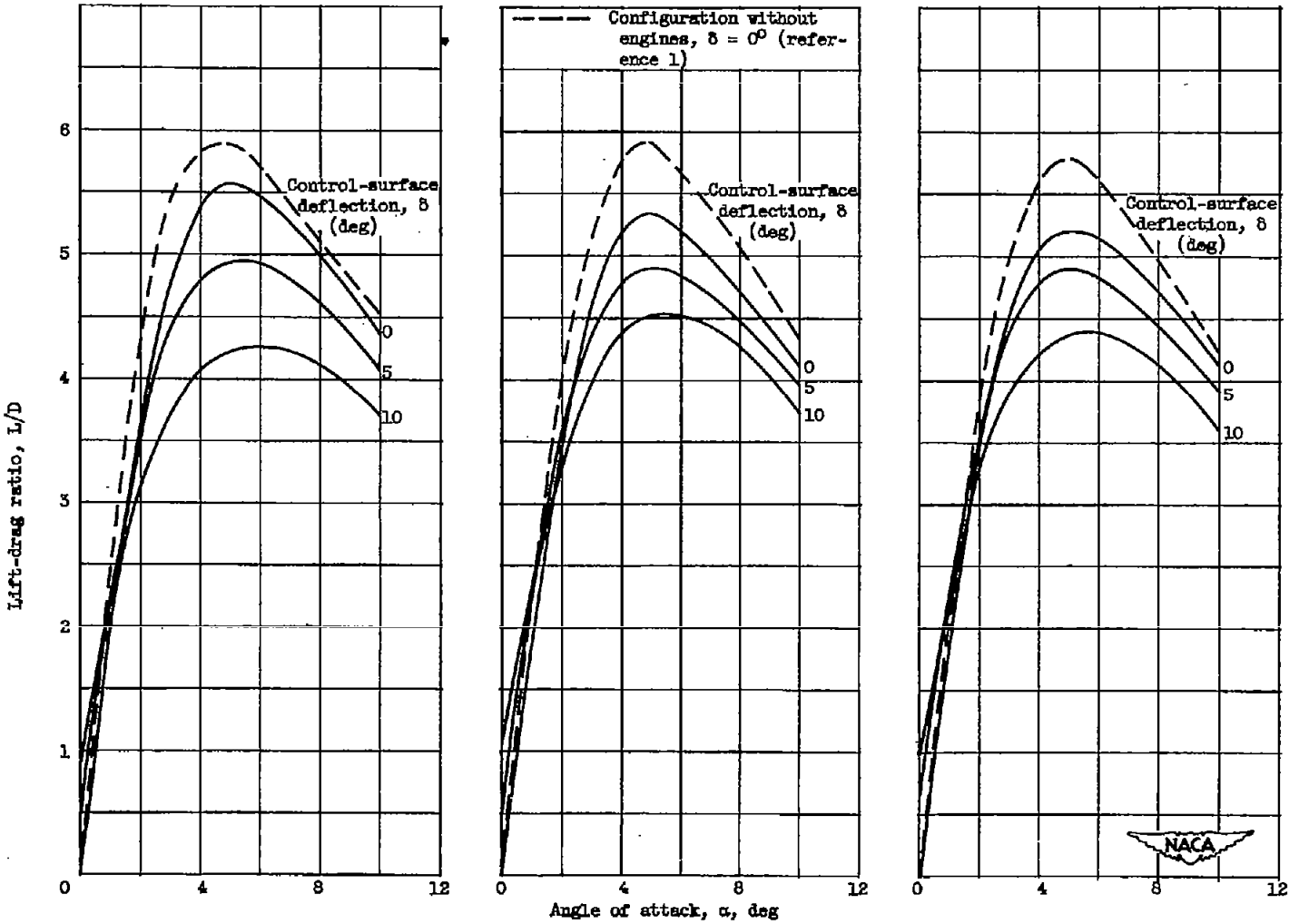

(a) $M_0 = 1.5$. (b) $M_0 = 1.8$. (c) $M_0 = 2.0$.

Figure 8. - Variation of configuration lift-drag ratio with angle of attack for several control-surface deflections and three Mach numbers. (Supercritical inlet operation.)

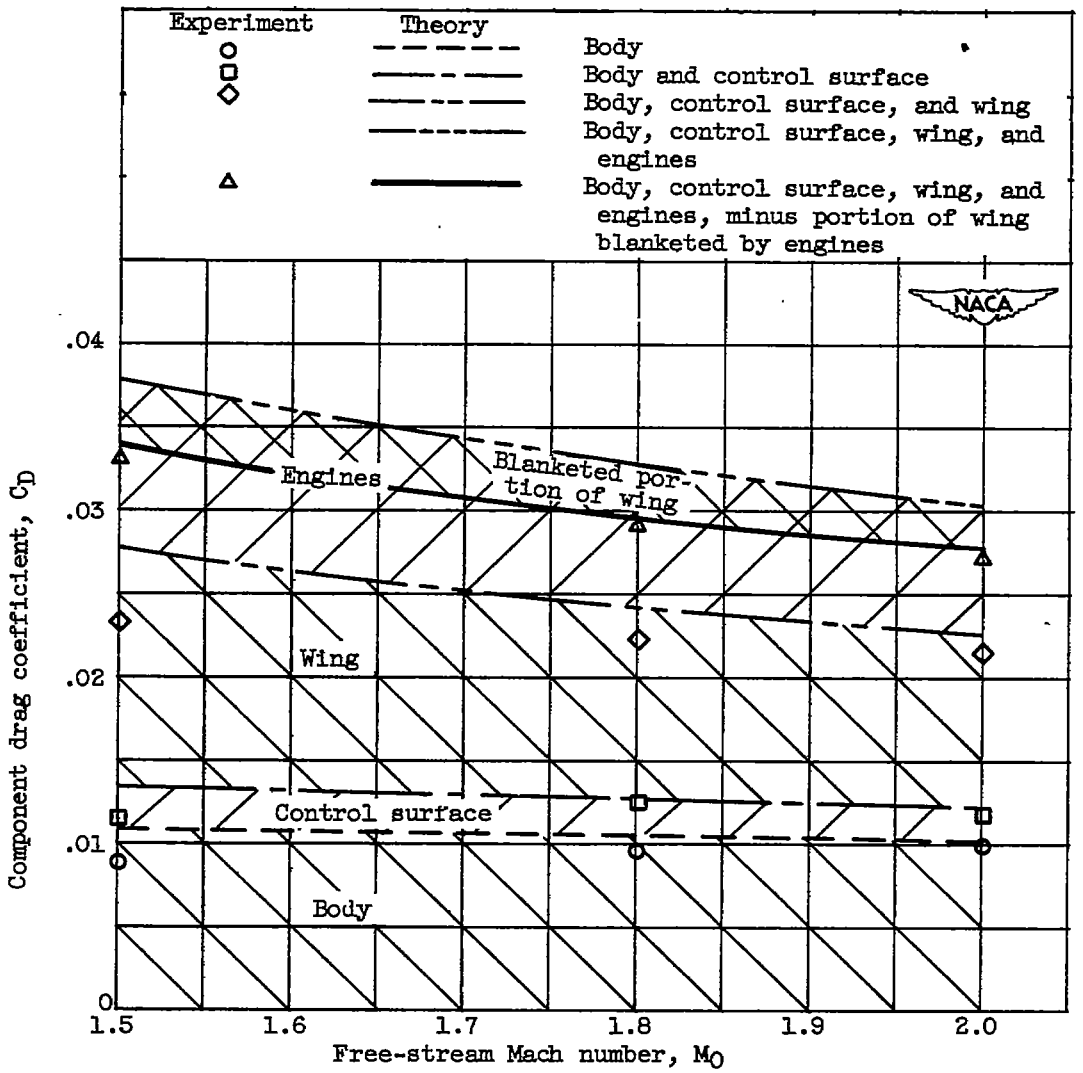

Figure 9. - Variation of experimental and theoretical component drag coefficients with free-stream Mach number at zero angle of attack and zero control-surface deflection. (Supercritical inlet operation.) (Reference 1.)

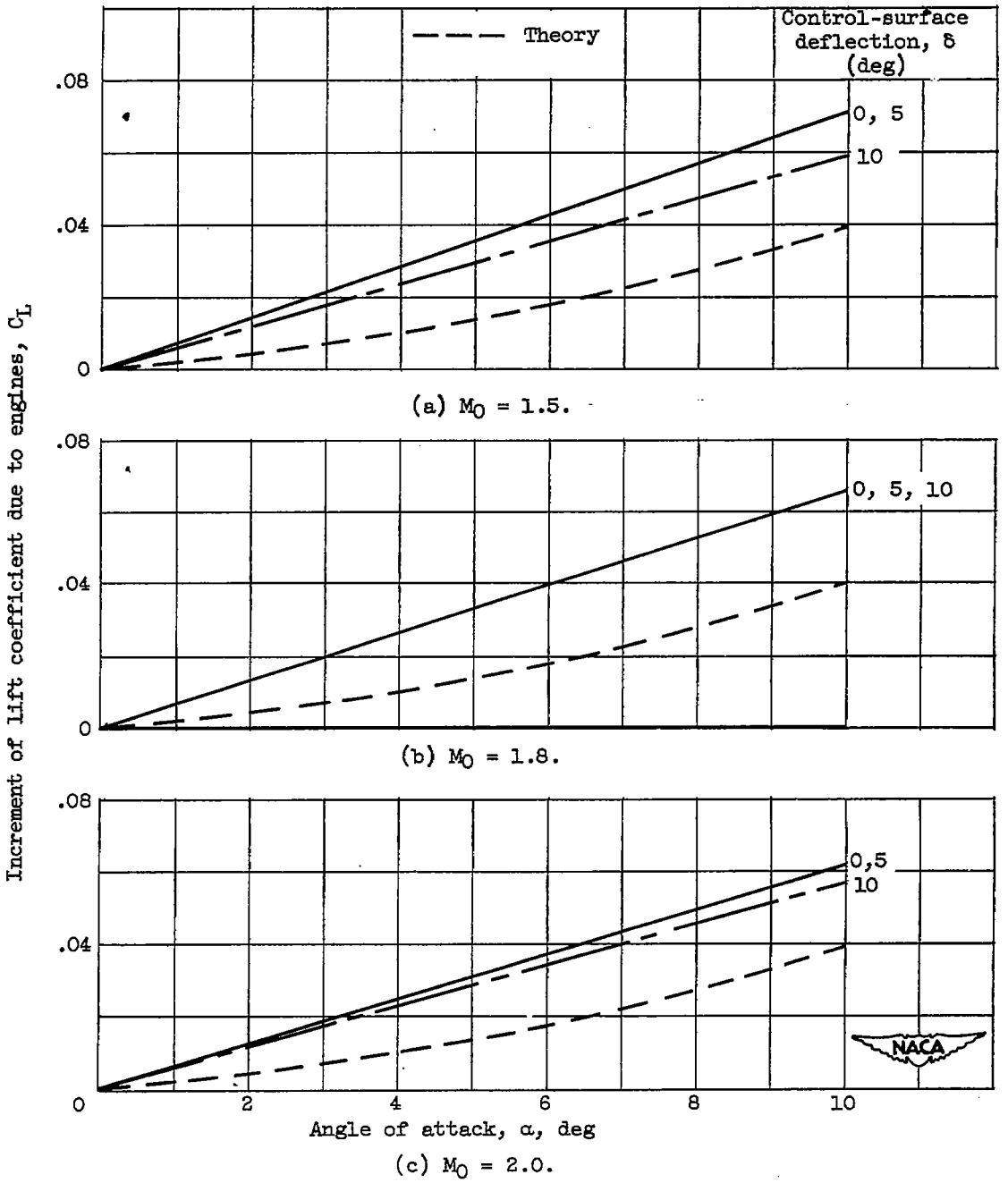

Figure 10. - Variation of increment of lift coefficient due to engines with angle of attack for several control-surface deflections and three Mach numbers. (Supercritical inlet operation.)

[redacted]

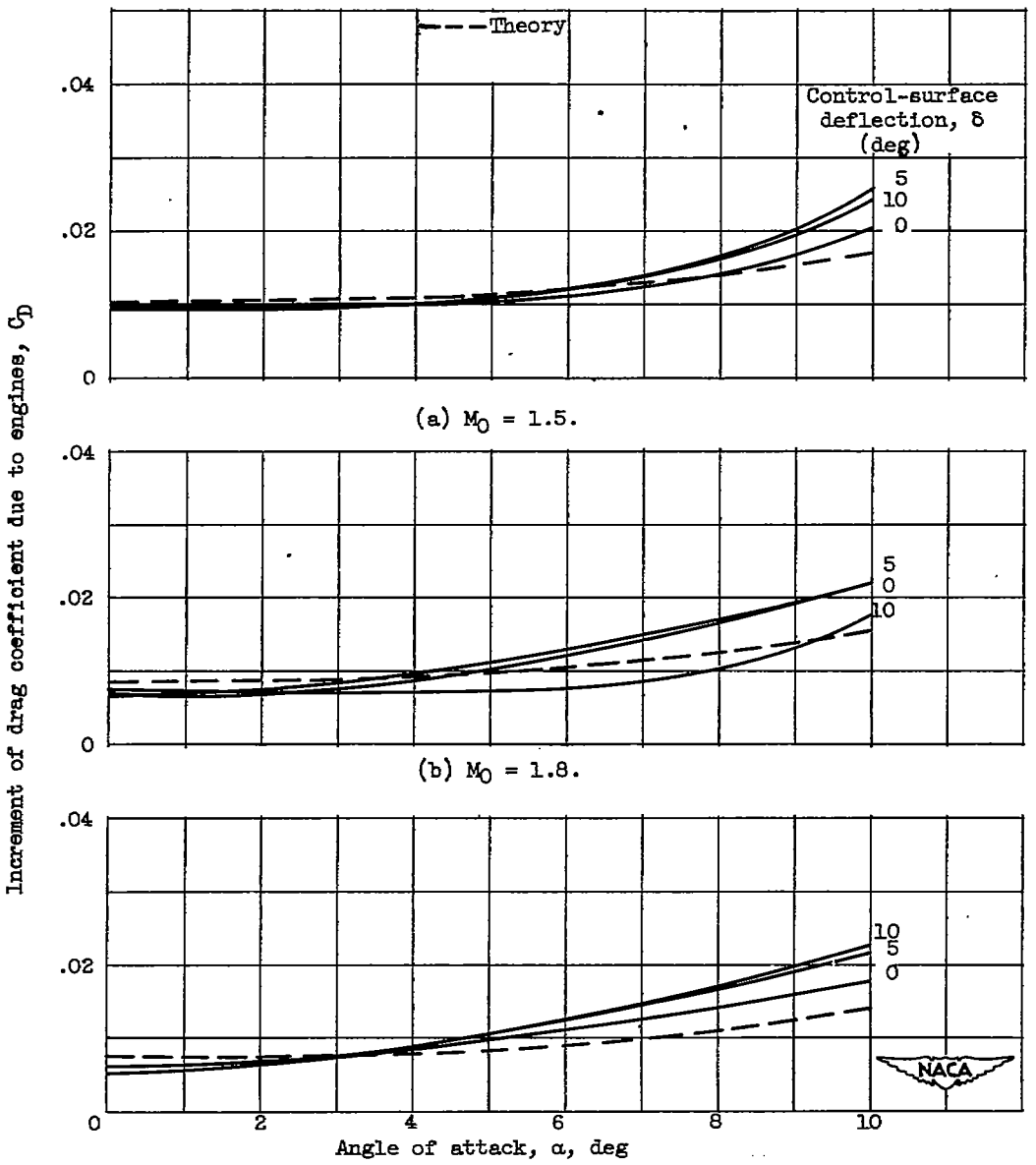

Figure 11. - Variation of increment of drag coefficient due to engines with angle of attack for several control-surface deflections and three Mach numbers. (Supercritical inlet operation.)

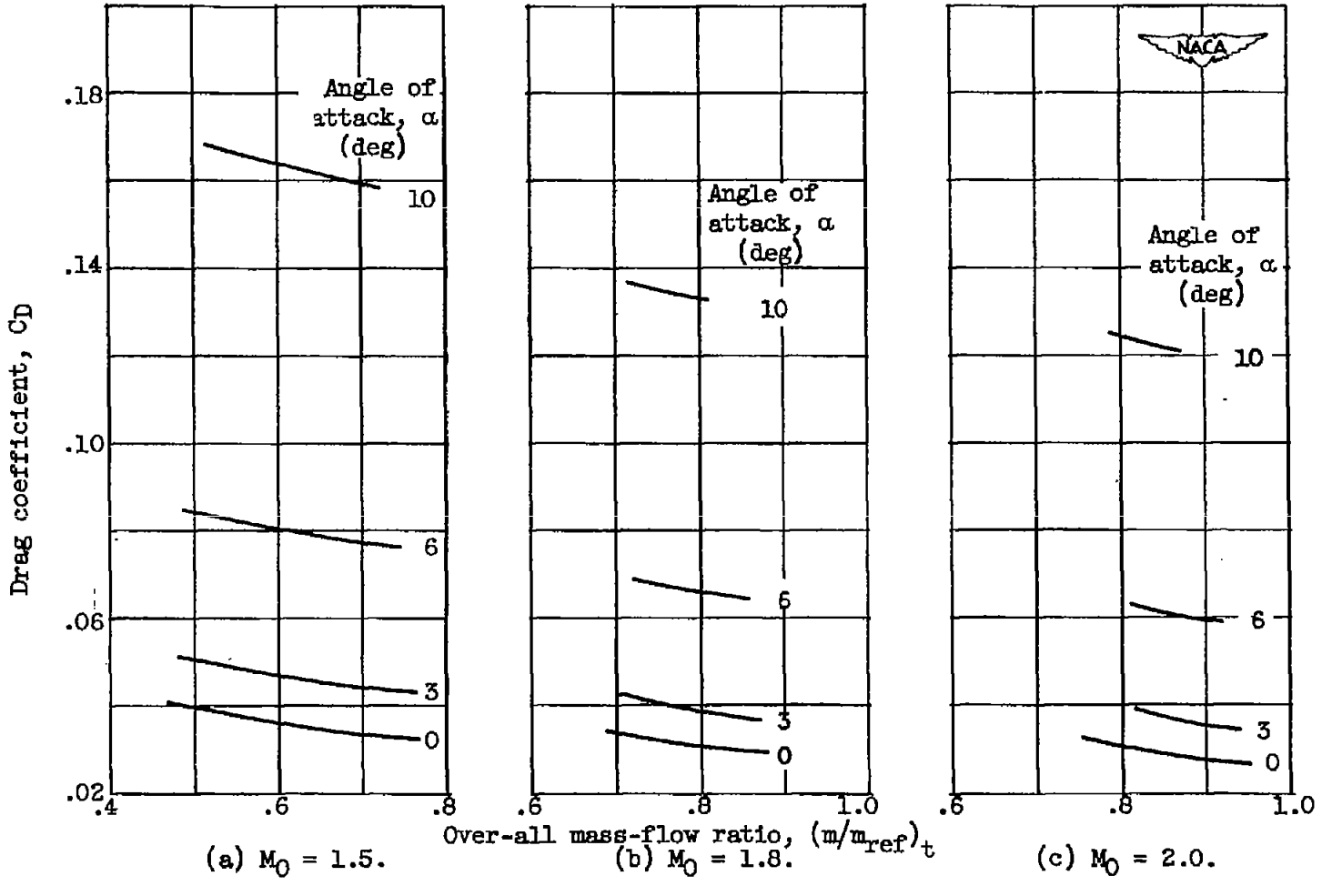

Figure 12. - Configuration drag coefficient as function of over-all mass-flow ratio. Zero control-surface deflection.

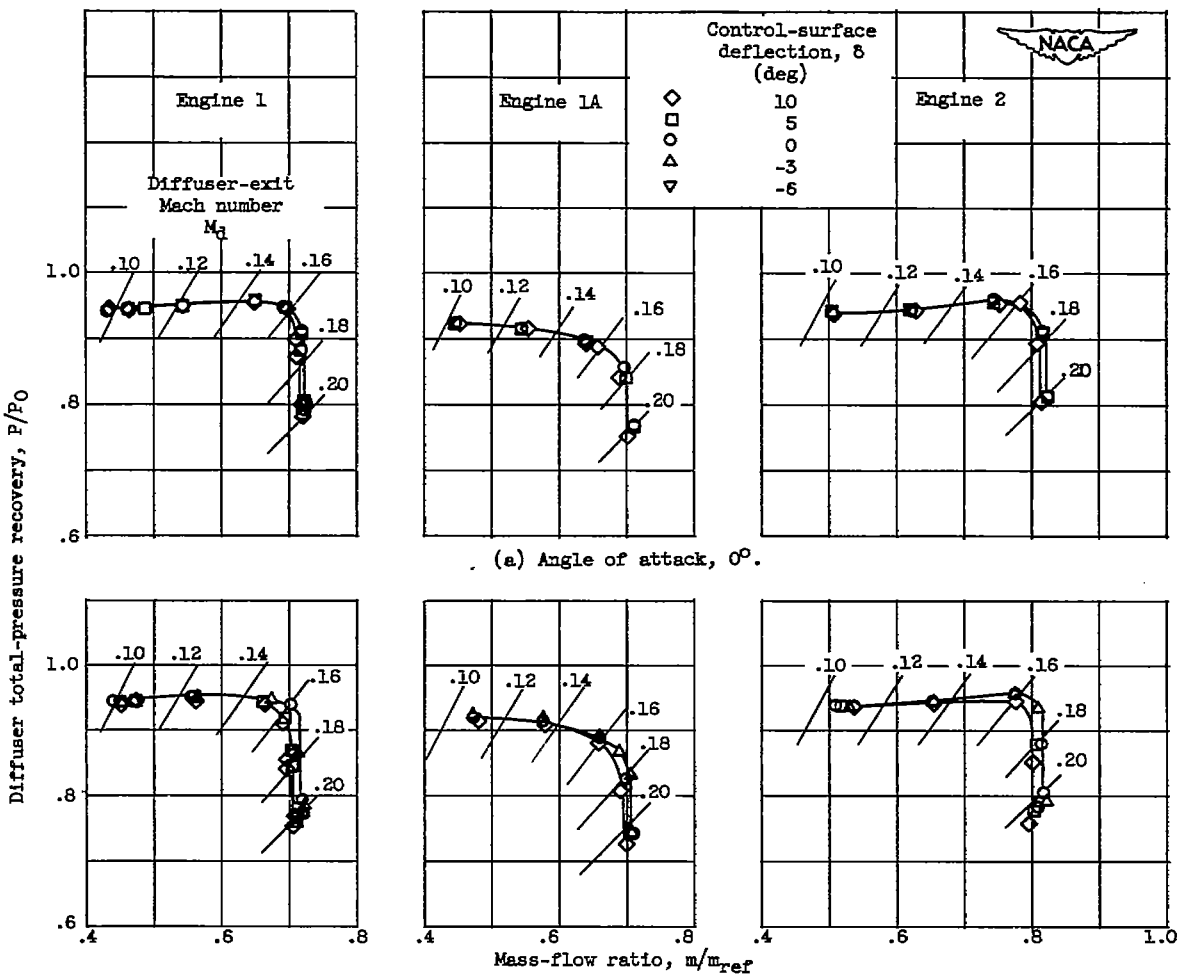

(a) Angle of attack, 0°.

(b) Angle of attack, 3°.

Figure 13. - Variation of total-pressure recovery with mass-flow ratio at Mach number 1.5.

[redacted]

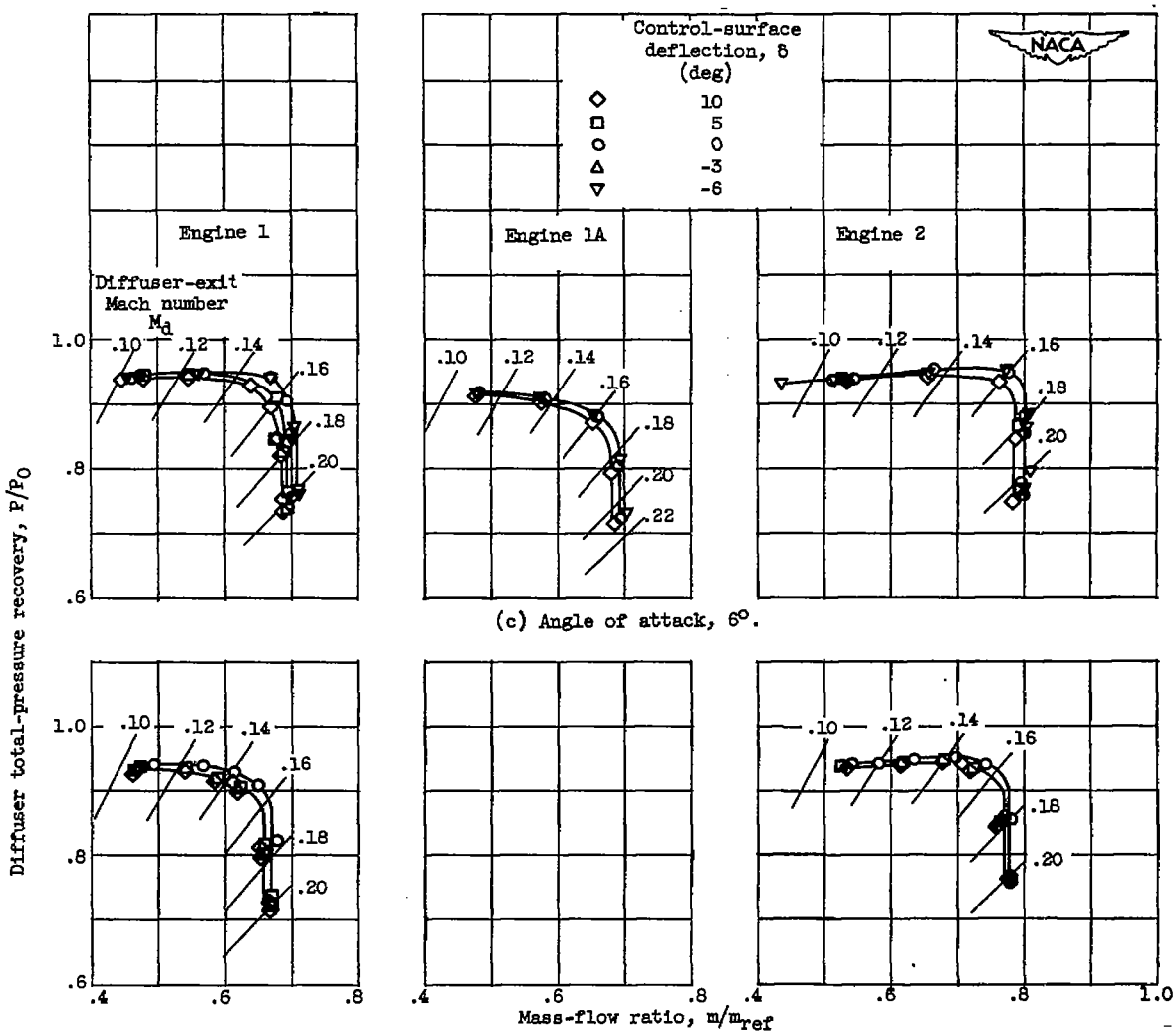

(c) Angle of attack, 6°.

(d) Angle of attack, 10°.

Figure 13. - Concluded. Variation of total-pressure recovery with mass-flow ratio at Mach number 1.5.

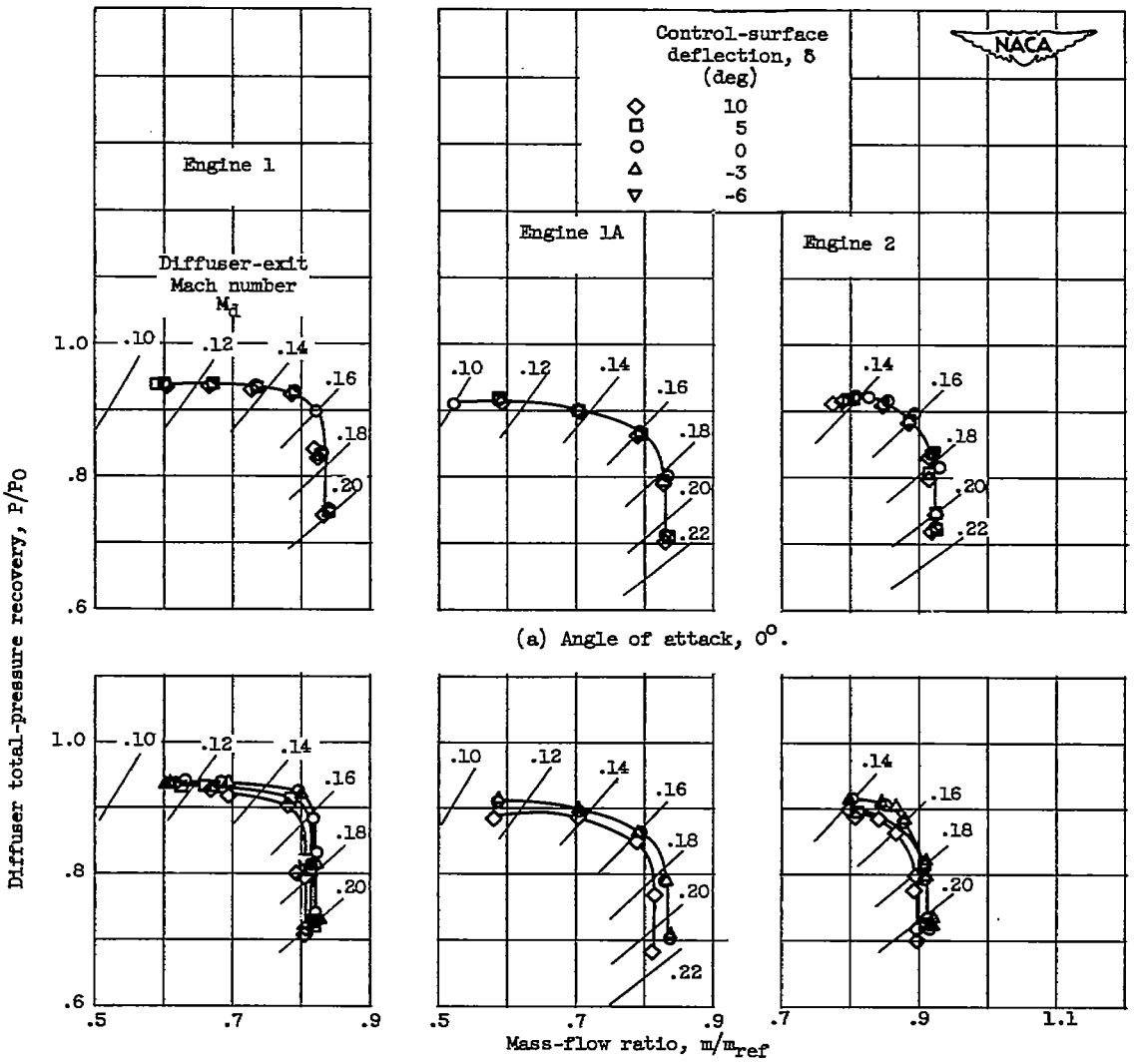

(a) Angle of attack, 0°.

(b) Angle of attack, 3°.

Figure 14. - Variation of total-pressure recovery with mass-flow ratio at Mach number 1.8.

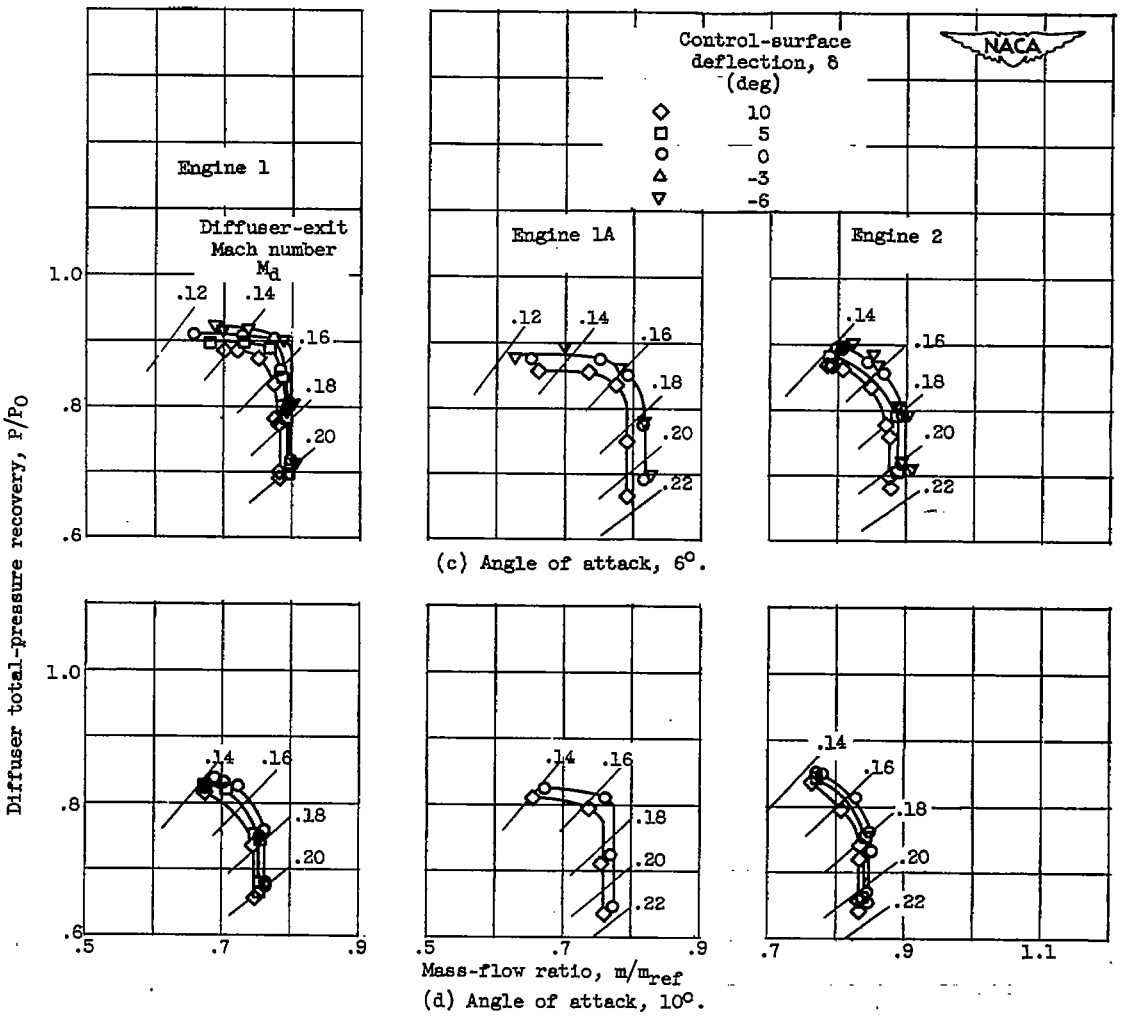

Figure 14.- Concluded. Variation of total-pressure recovery with mass-flow ratio at Mach number 1.8.

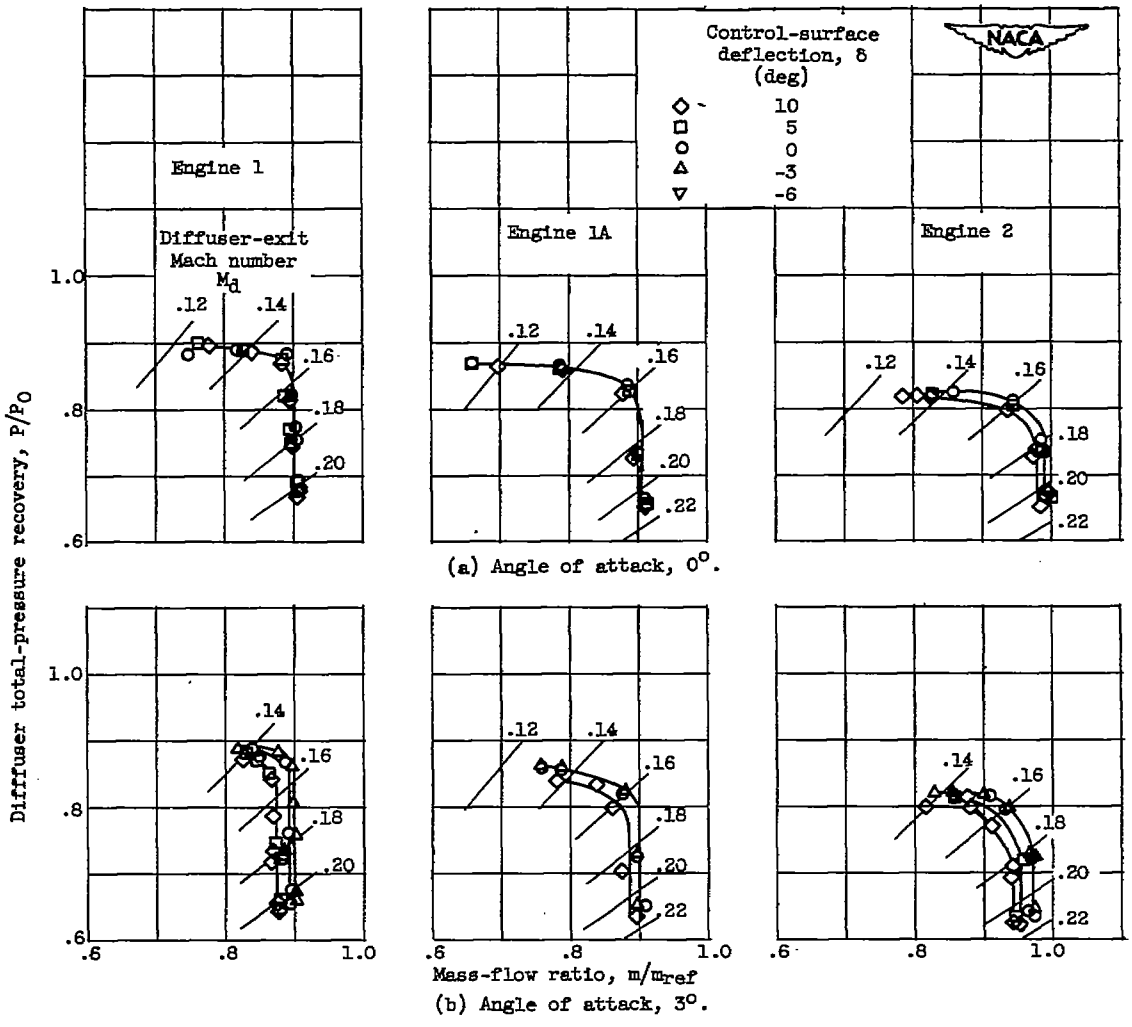

(a) Angle of attack, 0°.

(b) Angle of attack, 3°.

Figure 15. - Variation of total-pressure recovery with mass-flow ratio at Mach number 2.0.

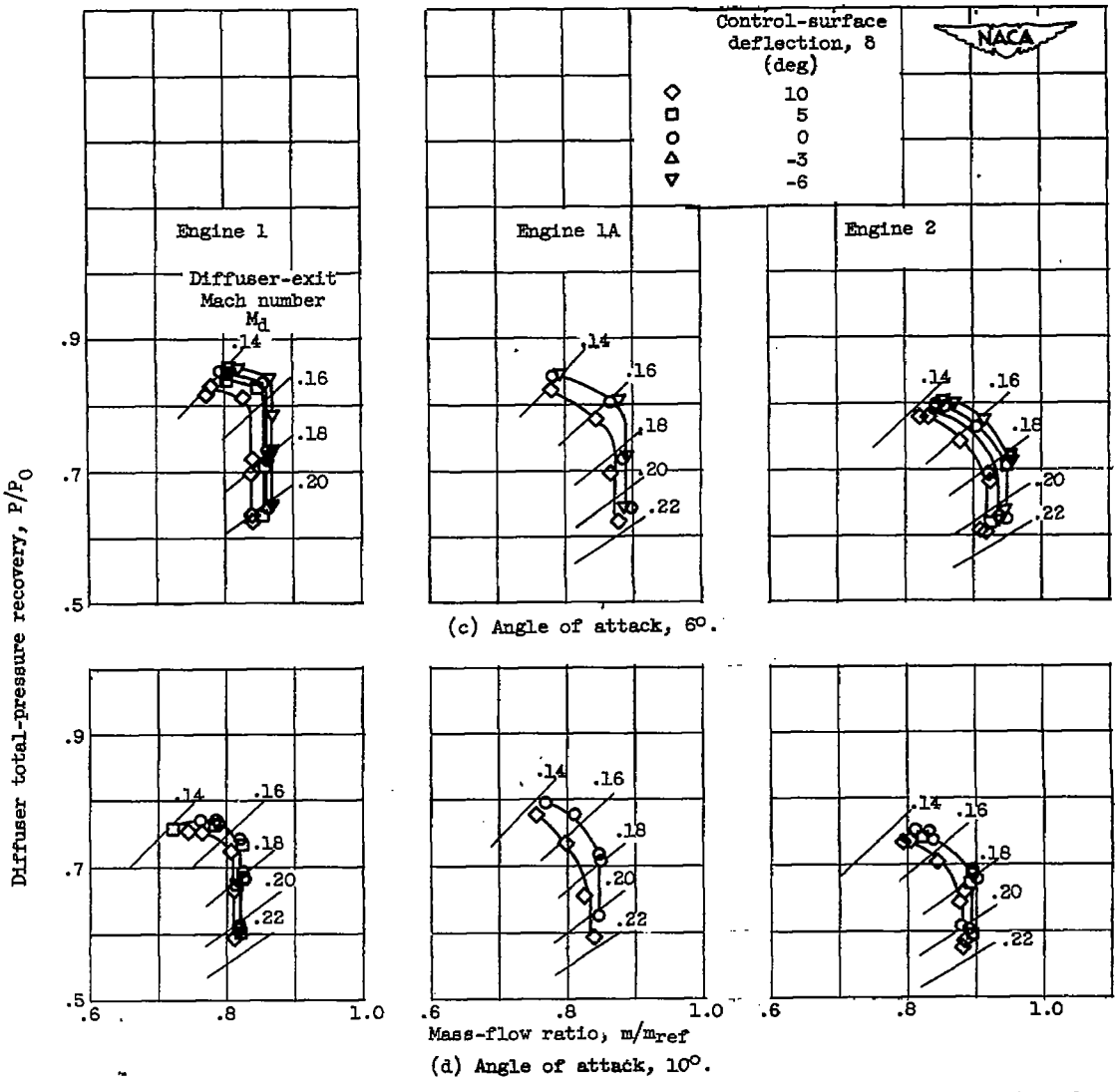

(c) Angle of attack, 6°.

(d) Angle of attack, 10°.

Figure 15. - Concluded. Variation of total-pressure recovery with mass-flow ratio at Mach number 2.0.

NACA-Langley - 11-24-52 - 400